Prepared for the National Institutes of Health
National Institute of Neurological Disorders and Stroke
Division of Stroke, Trauma and Neurodegenerative Disorders
Neural Prosthesis Program
Bethesda, MD 20892

Microstimulation of the Lumbosacral Spinal Cord: Mapping

NIH-NINDS-NO1-NS-8-2300

Quarterly Progress Report #7

Period Covered: 1 April, 2000 - 30 June, 2000

Principal Investigator: Warren M. Grill, Ph.D.

Co-Investigators: Kenneth J. Gustafson, Ph.D.
Musa A. Haxiu, M.D., Ph.D.
Michel A. Lemay, Ph.D.

Department of Biomedical Engineering
Case Western Reserve University
Cleveland, OH 44106-4912

ABSTRACT

The objectives of this research are to determine the anatomical locations of spinal neurons involved in control of the genitourinary and hindlimb motor systems, and to determine the physiological responses evoked in the genitourinary and hindlimb motor systems by intraspinal microstimulation. During this quarter we made progress toward both of these objectives. We began a series of experiments using intraspinal injections of retrograde tracers to identify last-order interneurons that project to either the preganglionic innervation of the bladder or the pudendal motoneurons innervating the external urethral sphincter. Secondly, we continued our experiments measuring the hindlimb motor responses evoked by intraspinal microstimulation. In these experiments we extended our previous static measurements to quantify the hindlimb motion generated by microstimulation of the lumbar spinal cord.

INTRODUCTION

Electrical stimulation of the nervous system is a means to restore function to individuals with neurological disorders. The objective of this project is to investigate the feasibility of neural prosthetics based on microstimulation of the spinal cord with penetrating electrodes. Specifically, chemical and viral retrograde tracers, immediate early gene expression, and immunocytochemistry are used to determine the locations and neurochemical identity of neurons in the spinal cord that control genitourinary and motor functions in the male cat. Microstimulation with penetrating activated iridium microelectrodes is used to determine the physiological effects in the genitourinary and motor systems of activation of different neural populations. Finally, inverse potential mapping is being explored as a method to determine, via spinal surface potential recordings, the location of active populations of neurons. The results of this project will provide data important to understanding neural control of genitourinary and motor functions, answer fundamental questions about microstimulation of the spinal cord, and lead to development of a new generation of neural prosthetics for individuals with neurological impairments.

PROGRESS IN THIS QUARTER

During the seventh quarter of this contract we began a series of experiments using intraspinal injections of retrograde tracers to identify last-order interneurons that project to either the preganglionic innervation of the bladder or the pudendal motoneurons

innervating the external urethral sphincter. Secondly, we continued our experiments measuring the hindlimb motor responses evoked by intraspinal microstimulation.

Identification of Last-Order Genitourinary Interneurons

The objective of these experiments is to identify the location and rostrocaudal extent of last-order premotor interneurons that project to the pudendal motor nucleus. We used retrograde transport of fluorescent latex microspheres (Retrobeads, LumaFluor Inc., Naples, FL) and the beta subunit of cholera toxin (CTB) (List Biological Laboratories, Inc., Campbell, CA) injected into the pudendal motor nucleus to determine the distribution of last order neurons projecting to the motoneurons innervating the external urethral sphincter. Two survival experiments and one post-mortem cat experiment were conducted with post-injection survival times of 44 and 60 hours.

Methods

Animal Preparation: All animal care and experimental procedures were according to NIH guidelines and were reviewed and approved by the Institutional Animal Care and Use Committee of Case Western Reserve University. Experiments were performed on adult male cats (4.1-5.3 kg). Animals were anesthetized with ketamine hydrochloride (35 mg/kg, IM) and given atropine sulfate (0.05 mg/kg, IV), gentamicin (25 mg, IV, every 12 hrs and dexamethasone (2 mg/kg, IV). The cephalic vein was catheterized and subsequent anesthesia maintained with sodium pentobarbital (2-3 mg/kg/hr, IV). Animals were intubated and mechanically ventilated with room air and supplemental oxygen as needed. A urethral catheter was placed and the bladder allowed to empty. End-tidal CO_2, heart rate, and oxygen saturation were monitored. The carotid artery was cannulated and arterial blood pressure monitored. Animal core temperature was maintained between 37°-39° C using a thermostatically controlled heating pad and heat packs. Saline and Ringer's solution, each containing $NaHCO_3$ (0.84%) and glucose (5%) were alternately administered throughout the procedure (10-20 ml/kg/hour, IV).

A laminectomy was made to expose spinal cord; segments L5-S1 were removed. The right pudendal nerve was isolated, verified by stimulation, placed on hook electrodes, and covered with mineral oil. Each animal was mounted in a stereotaxic frame.

Tracer injection location: The location of the pudendal motor neuron population was identified both anatomically and electrophysiologically. The L7, S1, and S2 segment exit sites were located, the roots identified and the dorsal rootlets traced back to the spinal cord to define the segments with respect to the spinal cord. The approximate center of the urethral sphincter motorneurons population lies in Onuf's nucleus at the caudal end of

the S1 segment, at the ventral edge of the gray matter. [VanderHorst, 1997, Jankowska, 1993, Thor, 1989, Ueyama 1984, Nadelhaft, 1980].

The cord dorsum potentials (afferent activity evoked by stimulation of the pudendal nerve) were recorded with a silver ball electrode placed (~500 μm Diam.) at the midline or dorsal root entry zone. The peak of the cord dorsum recordings was used to determine to rostral-caudal location for field potential injections.

Extracellular antidromic field potentials within the spinal cord evoked by stimulating the pudendal nerve branch (200 μsec stimuli at 2 Hz, Pulsar stimulator, FHC, Inc., Bowdoinham, Maine) were recorded with a tungsten microelectrode (75μm Diam., 300-500 kΩ, FHC, Inc., Bowdoinham, Maine), amplified (Grass P511 AC amplifier), averaged, and displayed on an oscilloscope. Multiple penetrations were made starting at the dorsal root entry zone to locate the peak of the ventral field potentials. Electrode depth was controlled with a microdrive unit (Transvertex, Stockholm, Sweden).

The platinum ball electrode, microelectrode and micropipette were each mounted in identical glass micropipette tubing so each fit in the same holder fitting. This allowed the electrodes to be exchanged while maintaining the electrode position relative to the spinal cord.

Tracer injection: Two types of retrograde tracers were used: fluorescent latex microspheres (Retrobeads, LumaFluor Inc., Naples, FL), both rhodamine and green; and the beta subunit of cholera toxin (CTB) (List Biological Laboratories, Inc., Campbell, CA). Use of different tracers will allow us to identify premotor neurons which project to one, the other, or both nuclei. Tracers were loaded into calibrated glass micropipettes (Drummond Scientific Co., Broomhall, PA). The inner diameter (340 μm) of the calibrated pipettes was small enough to allow visualization of the tracer meniscus (1.10 mm per 100 nl) and therefore verification of injection volume. The pipettes were pulled and coated in silane (N,N - Dimethyltrimethylsilyamine, Fluka Chemicals) by twice dipping and heating at >150 C for one hour. This process gave the micropipette tip a hydrophobic coating that reduced tracer wicking along the micropipette after injection. The tips were then broken to a tip diameter of approximately 30 μm. The micropipette was backfilled with the tracer using a microfil syringe (WPI, Sarasota, FL).

Tracer loaded micropipettes were inserted into the spinal cord at the point determined from the electrophysiological and anatomical mapping, and advanced to the target population. A 5 min delay after at the location was allowed for the pipette to seal and reduce tracer wicking around the micropipette. Tracers were injected using a pneumatic picospritzer (Picopump, WPI, Sarasota, FL) driven by N_2 gas. Multiple pressure pulses were used (typically 10-30 psi; 100-200 msec) to inject 300 to 600 nl of each tracer. Injected volumes were verified by visualization of the tracer meniscus. Individual pulses were limited to approximately 10 nl and a 3 min pause was used after

injection of each 100 nl. Rhodamine and green microspheres were injected in identical locations (lateral distance and depth) on opposite sides of the spinal cord and CTB injected in the same location a few mm rostral. A 10-minute delay after injection and a very slow withdraw of the micropipette was used to maintain tracer location.

After tracer injection, the incisions were closed and the cats maintained on anesthesia and monitored continuously for 44-60 hours post injection. During this period, animals were turned regularly and blood pressure, end-tidal CO_2, heart rate, hydration and oxygen saturation were monitored. After the incubation period, the animals were perfused via the aorta with 1 liter of warm (37°C) heparinized saline followed by 2 liters of warm 4% paraformaldehyde in 0.1M $NaPO_4$ buffer (PBS, pH=7.4), followed by 2 liters of cold (5°C) 4% paraformaldehyde in PBS. Paraformaldehyde was selected as the fixative because glutaraldehyde degrades bead fluorescence [Hoover and Durkovic, 1992].

Tissue processing and analysis: The lumbosacral spinal cord was exposed and roots verified. The segments L3-S3 were cut, removed and post-fixed for 2 days in cold (5°C) 4% paraformaldehyde in PBS, followed by 2-4 days in 30% sucrose in PBS. The left dorsal side of the cord was nicked to mark side orientation. The lumbosacral cord was sectioned at 30μm intervals in the transverse plan on a freezing microtome, and a 1 in 5 series (each bin represents 0.15 mm of cord) of the sections mounted in serial order, counter-stained with neutral red, and coverslipped. A second section from each series was processed for immunocytochemical detection of CTB. Slides were viewed with a combination light/fluorescence microscope (Leitz Laborlux S). The injection sites were visualized and reconstructed, and the distribution of labeled neurons in the spinal cord identified. Selected cross sections of the spinal cord were digitzed at low magnification and printed to evaluate the rostrocaudal extent of labeled cells and allow cross sectional reconstructions of the injection sites.

Results and Discussion

Electrophysiological nucleus location: Cord dorsum potentials demonstrated a broad peak in the rostral S2 segment over a range of at least a few mm. Identification of the penetration location based on the cord dorsum potentials and anatomical landmarks were separated by 5 mm, which is within the rostral-caudal extent of the nucleus. The resolution of peak field potentials within the cord was insufficient to precisely determine the nucleus location within a penetration. Therefore injections were based on anatomical landmarks and not on direct field potential recordings. Stimulation of the whole pudendal nerve results in both afferent and efferent evoked field potentials. Stimulation of only the motor branch of the pudendal nerve will be used in future experiments to

improve the resolution of the field potential recording. In addition, selected sections from each experiment have been analyzed and combined with the literature to determine the expected range of the anatomical location within a penetration (also see injection site accuracy section below).

Injection site reconstruction: Histological analysis resulted in reconstruction of the injection sites, which is required to validate the experimentally intended injection site location (determined electrophysiologically and anatomically during the procedure). Comparison of the histologically observed injection site to the experimentally intended injection site evaluates the precision of the instrumentation. Comparison of the observed injection site to the expected pudendal motor nucleus location based on the literature is required to evaluate the accuracy of the approach and to relate retrograde labeled interneurons to the correct (urethral sphincter) motor nucleus.

Injection site precision

Each injection site could be identified histologically. The location of the rostral/caudal center of an injection site was determined from serial cross sections by the section with the maximum injection site (microsphere deposit) diameter. The rostral-caudal resolution was 150 _m (5 30 _m slices). Reconstruction of the injection sites matched the experimentally intended injection site locations. An example of a spinal cord cross-section showing the center of the rhodamine microsphere injection site in cat B002 is shown in Figure 1. The precision of the technique for this injection is acceptable, however the accuracy was not sufficient.

The center of the rhodamine injection site based on the microsphere evaluation (microsphere mark in Figure 1) was 85 _m medial and 500 _m deeper than the experimentally expected location (Experimental injection site mark in Figure 1). The experimentally intended site is at the top of the bead injection area; therefore it is possible that the beads were injected downward from the pipette location. Therefore the precision of the instrumentation and technique was adequate for this injection. The total volume of microspheres injected will be reduced to match the expected size of the urethral sphincter motor nucleus.

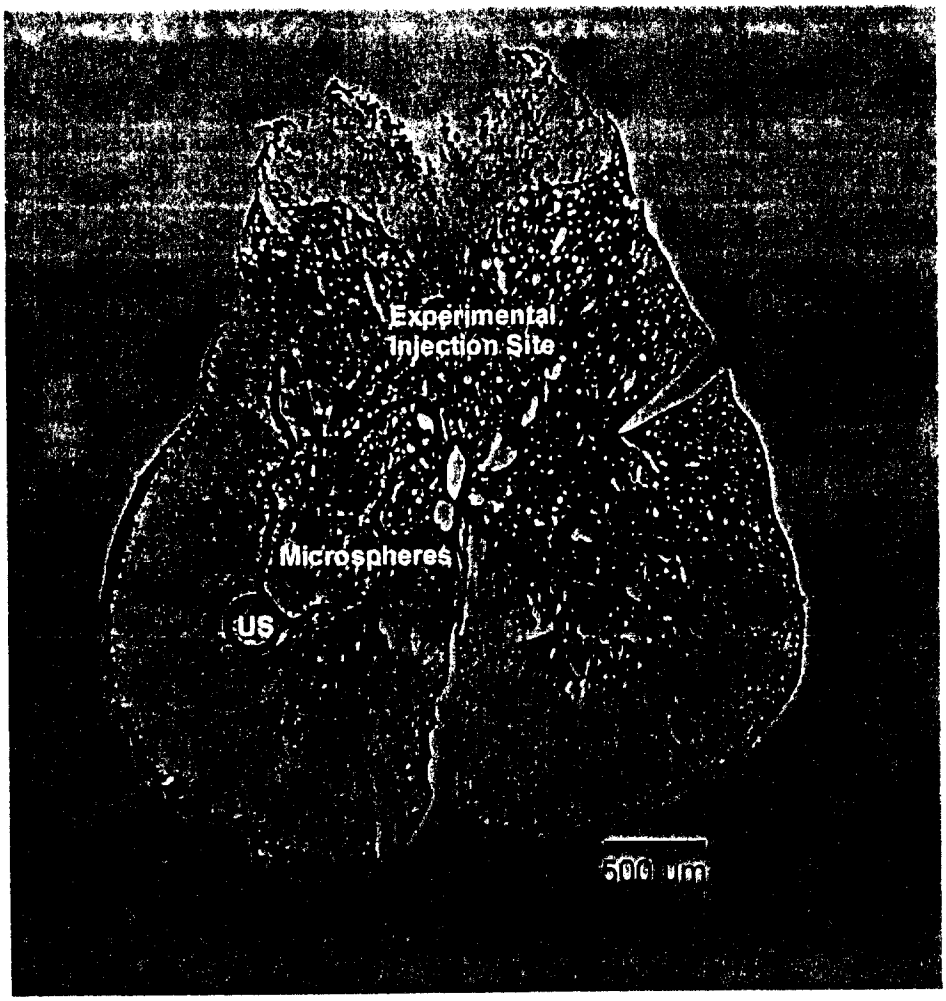

Figure 7.1. Spinal cord cross-section from the caudal S1 segment showing the center of the rhodamine microsphere injection site in cat B002. An outline of the microsphere spread of the injection site based on fluorescent microscopy is shown (Microspheres) and the center of the microsphere area marked. The experimentally intended injection site is also marked (Experimental injection site). Cross hair errors are ± 100 μm. The approximate location of the urethral sphincter motorneuron population (US) is shown for reference. The section has been reduced in size approximately 15% during histological processing. The urethral sphincter nucleus diameter and injection location dimensions were therefore reduced 15% for comparison on this figure.

In an additional animal, a number of injections were made post-mortem over of a range of locations and volumes. All injection sites were identified based on histological reconstruction. There was an approximate 2 mm shift in rostral caudal distances between post mortem labeling and histological reconstruction. All injection sites were less deep within the cord than expected. This was consistent with a relatively larger degree of cord dimpling observed in this post mortem experiment. The injection micropipettes have been modified to have a smaller profile and smaller diameter (30 to 50 μm) tips. These changes have reduced the dimpling effect.

Injection site accuracy

Although the injection areas matched the experimentally intended locations, they were not consistent with the expected center of the pudendal motor nucleus. As shown in Figure 1, the rhodamine bead injection site in cat B002 is dorsal and medial of the expected urethral sphincter motor nucleus location. The green bead injection site of cat B002 was approximately in the middle of the medial ventral horn, centered in lamina VII. The edge of the injection site may have included a small amount of the pudendal nucleus area, however it is unlikely that any of the retrograde labeled cells from this injection represent the urethral sphincter nucleus. As discussed in the electrophysiological nucleus location section, improved field potential recordings will improve the accuracy of the injection site placement. It is expected that selective stimulation of the urethral sphincter motor branch instead of the whole pudendal nerve will increase resolution of the urethral sphincter evoked field potentials since there will be no afferent neurons activated. In cat B001, the microsphere injection site was outside the gray matter; therefore no retrograde transport of beads was observed.

Injection site volumes

Injection volumes were estimated based on the diameter of the circular microsphere area resulting from the injection site within a spinal cord cross-section. Serial sections were utilized to estimate the rostral-caudal distribution of an injection site. The rostral-caudal resolution was 150 μm (5 30 μm slices). The injection site shapes were not completely circular and there was some degree of spread, therefore the diameter was estimated. In cat B002, the injection sites were approximately spherical and the estimated volumes based on the histology serial sections match the rhodamine-injected volume (see Figure 1), however are only approximately half of the green injected volume. The injection sites in the post mortem animal were extended in the rostral-caudal direction and shaped similar to an ellipsoid. The volume estimates ranged within approximately 30% of the predicted volume.

Labeled cell analysis and interneuron identification: Retrograde labeling of spinal neurons from both rhodamine and green fluorescent microspheres injection sites was observed in cat B002, demonstrating the feasibility of using latex microspheres for retrograde labeling of premotor neurons. Although the injection sites in cat B002 did not overlap the urethral sphincter motor nucleus, identifying the retrograde labeled cells and relating them to cells at the injection site may still yield valuable information. For example, the bladder is innervated by parasympathetic preganglionic efferent neurons in a slender 10 mm columnar nucleus extending from S1 to S3 with the density the highest in S2 [Nadelhaft et al., 1980, Ueyama et al., 1984]. These cells lie vertically at the lateral

edge of the gray matter in laminae V-VII, in what is termed the lateral band of the sacral parasympathetic nucleus [Nadelhaft et al., 1980]. This area overlaps with the rhodamine injection site area in cat B002.

Analysis of the retrograde labeled cells is ongoing, however an initial analysis of the labeled cells in cat B002 has been performed. As expected, there were no labeled cells in the S2 or S3 segments, therefore no anterograde labeling was observed. The distribution and intensity of retrograde labeled cells varied within and between segments. The majority of rhodamine labeled cells was in the L6 segment, where labeled cells were observed across a large laminar distribution.

Rate of retrograde transport: The observed retrograde transport indicates that the microspheres can be transported over several segments within the post-injection survival period. The rostral labeling observed in cat B002 was used to determine the minimum rate of retrograde bead transport. After a post injection time of ~ 60 hours, the farthest rostral point from the injection site that microspheres were observed was in the L4 segment, 32 mm rostral from injection site (S1 segment). These microspheres were observed in the medial edge of lamina VII or VIII. Therefore the transport rate was at least 0.5 mm/hour. Retrograde transport occurs at a rate greater than 10 mm/hour [Nicholls et al., 1992], but is slowed by anesthetics. The minimum observed rate of 0.5 mm/hour is less than the expected conservative estimate of 1 mm/hour. The labeled section in the L4 segment may have been the farthest rostral projection from the injection site, therefore, the experimental rate of retrograde transport may have been greater than the minimum observed rate of 0.5 mm/hour.

Summary of key findings: Retrograde labeling of spinal neurons from fluorescent microsphere injection sites was observed, demonstrating the feasibility of using latex microspheres for retrograde labeling of premotor neurons. The minimum observed rate of retrograde transport was 0.5 mm/hr. Injection sites were reconstructed from histological sections, and the precision of the injection technique is adequate. The field potential recordings must be improved to obtain sufficient injection site accuracy.

Dynamic Hindlimb Motor Responses Evoked by Intraspinal Microstimulation

During this quarter, we extended our previous studies of the endpoint forces evoked by microstimulation of the lumbar spinal cord to include hindlimb motion evoked by intraspinal microstimulation. Surgical techniques were identical to the ones reported in earlier reports, but the robotic system described in previous reports was used to acquire the forces and motions. A brief description of the surgical methods will be given in the following paragraph, followed by a description of the new experimental robotic set-up.

Experimental set-up

The animal was anaesthetized with ketamine (25 mg/kg), and anesthesia maintained using halothane. A laminectomy was performed to expose the lumbar area of the cord (L4-L7), and the contralateral limb denervated by transection of the proximal sciatic, femoral, and obturator nerves. After the animal was transferred to a stereotaxic frame, a midcollicular decerebration was conducted and halothane anesthesia discontinued. The dura was opened to allow identification of the spinal roots. Cord and core temperatures are maintained at 36°C, and the cord was bathed in mineral oil. Blood pressure and expired CO_2 were monitored throughout the experiment.

The animal's pelvis was held with bone pins, and the paw attached to a gimball mounted on a six-axis force transducer. The force transducer was mounted at the end-point of the two-DOF robot described in a previous quarterly report. The robot can hold the paw isometrically during force measurements or be free-moving during motion measurements. The femur is no longer held and the hindlimb thus becomes a three link assembly, which allows for hip motion in addition to knee and ankle.

Fine bipolar wire electrodes were inserted into four hindlimb muscles (knee flexor, knee extensor, ankle flexor, and extensor) to record the electromyographic (EMG) activity simultaneously with forces and/or motions. The raw EMG signal was amplified, filtered (10-1000Hz), and sampled at 2000Hz.

Force and Motion Measurements

Motor responses were elicited by microstimulating the cord intraspinally with trains of biphasic current pulses (train duration: 0.5 s, frequency: 40Hz, pulse duration: 100μsec, pulse amplitude: 100μA). The cord was mapped by measuring responses along dorso-ventral penetrations in increments of 200μm, at a series of positions along the rostro-caudal medial-lateral surface of the cord. At selected depths for each of the penetration the limb was moved on a 3cm grid of nine to twelve points from a mid-stance position while stimulation parameters and electrode position are kept constant. The hindlimb's end-point is moved to each of the positions on the grid by the robot, and held isometrically (stiffness: 400-450 N/m) for the duration of the trial (typically three seconds).

The forces measured at those nine to twelve locations are used to calculate the forces acting on the limb's end-point throughout that workspace. The workspace is divided into triangles, and the forces within a triangle are estimated by a linear interpolation based on the three vectors measured on the vertices (see Fig. 7.2). The forces are divided into a passive component (force measured before the onset of activation), and an active component (total forces measured minus the passive portion). Total, active and passive force fields are reconstructed.

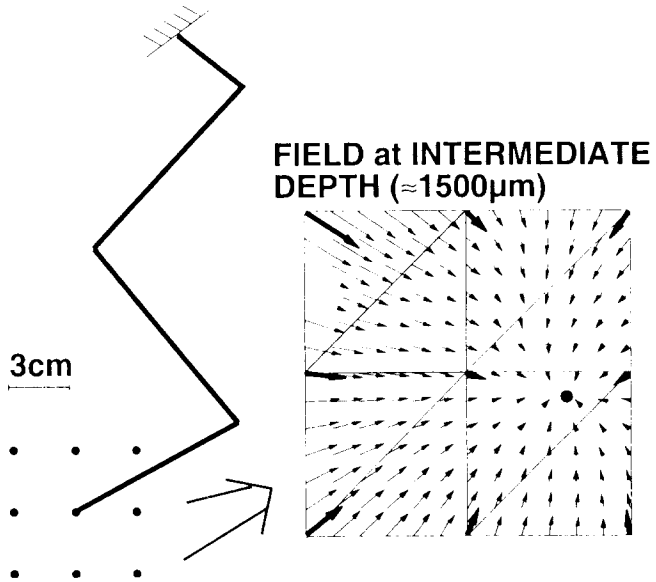

Figure 7.2 Force field construction. Left: spatial end-point locations where forces are recorded. The paw is moved to each of the location on the 3 cm grid with the pelvis held fixed via pins. The hip, knee and ankle are thus moved through varying range-of-motion, with the robot planar architecture preventing movements outside of the sagittal plane. Right: actual force vectors measured (thick dark vectors), triangles dividing the workspace, and the interpolated force vectors (thin light vectors). Forces represented are the total forces (active and passive).

Once the isometric forces produced by a particular spinal site were characterized, we measured the hindlimb movement produced by activation of the site. For motion measurement the robot's motors were programmed to counterbalance the weight of the linkages, thereby minimizing the apparent weight of the mechanical structure on the animal's hindleg. The action of gravity on the limb's weight was not compensated, and thus the leg started from a fully extended position prior to onset of stimulation.

We also evaluated movements accomplished against programmed springs of varying stiffnesses (range 25-200 N/m). Springs were implemented via the robot controller with the center of the spring typically programmed to be at the mid-stance

position, and the restoring force programmed to be that of a two dimensional linear stiffness spring, i.e. $F=K(X_D-X)$.

RESULTS

The results reported here were collected over two experiments, both using the decerebrate preparation described above. A total of 10 dorsoventral penetrations were performed (8 ipsilateral, 2 contralateral), and fields were collected at 10 selected depths. Only two of the previously described force patterns were obtained in these two experiments. Six of the ten fields were flexion withdrawal, and the remaining four were caudal extension response. We did not obtain rostral extension or rostral flexion responses. The absence of rostral flexion is easily explained by the relative paucity of the type: 1 out of 80 fields in all mapping experiments. Most of the penetrations in these experiments were ipsilateral to the limb, and since the relative occurrence of rostral extensor is only 6% for ipsilateral penetrations, the absence of rostral extension responses was not that surprising.

It is worth noting that the force patterns found did not change, even though the limb mechanical configuration changed significantly with the removal of the femur restraint. The limb is now a system of three links. Motion is limited to the animal's sagittal plane by the robot, but the joints' angles can no longer be calculated from inverse dynamics since the limb can now assumed the same end-point position with various combinations of knee, joint and hip angles. Since we can no longer obtain joint angles from the end-point position, we cannot calculate the joint torques in this arrangement. We have secured a digital video camera that will allow us to obtain the joint angles. Since the relationship between joint torque and end-point force ($T = J^T F$) is still valid, we will be able to obtain the torques evoked at the hip, knee and ankle by intraspinal microstimulation.

We measured the movements produced by five of the isometric force patterns reported above. Four of the patterns were flexor withdrawals, and one was a caudal extension. We evaluated the paw lifting ability of the flexor withdrawals, and we evaluated the extensor response against the robot programmed to behave as a linear spring holding the limb at the mid-stance position. We also evaluated a number of the flexor withdrawal responses against the simulated linear spring.

Since the duration of stimulation (0.5 s) used to generate the isometric forces was often too short to cause any significant movement, we increased the duration of the stimuli train (range 3-5 s) and verified that the active forces produced were larger but in the same orientation (at the mid-stance position). The forces were then sufficiently high and sustained to produce significant motion. Figure 7.3 depicts the total force field (for the 0.5 s duration train of pulses), as well as the movements evoked by a 3 s duration

stimuli train against three springs of increasing stiffness (spring desired position indicated by an X). The forces lift the leg and extend it backwards in the initial portion of the move, and the spring's action return the leg towards the center in the second portion of the movement. The large flexion withdrawal was evoked using a 5 seconds stimulation duration train of pulses. The robot was programmed to compensate for its own weight, and the active forces were sufficient to lift the entire leg against gravity towards a caudal flexed posture.

Figure 7.4 presents another example of leg motion against simulated two-dimensional springs, but for an extensor field. The figure depicts the total peak force field, and movements against one 50 N/m spring centered at (0 cm, 22 cm), and two 25 N/m springs centered at (0 cm, 22 cm) or (0 cm, 25 cm) (lower and higher traces respectively). As with the flexor field, the movement is in the direction of the forces evoked by the microstimulation. The limb extends backwards in the direction of the forces, and returns to the balance position between the upward pull of the spring and the gravity downward pull of the limb once stimulation terminates. Overall, both sets of results indicate that the direction of the forces measured isometrically are not drastically modified by limb movements. Further investigation into the dynamics of movements is required before we can determine if the isometric forces acting on a biomechanical model of the hindlimb including passive properties are sufficient to predict the movements, or if the forces applied to the limb during motion are affected by the dynamics of the move.

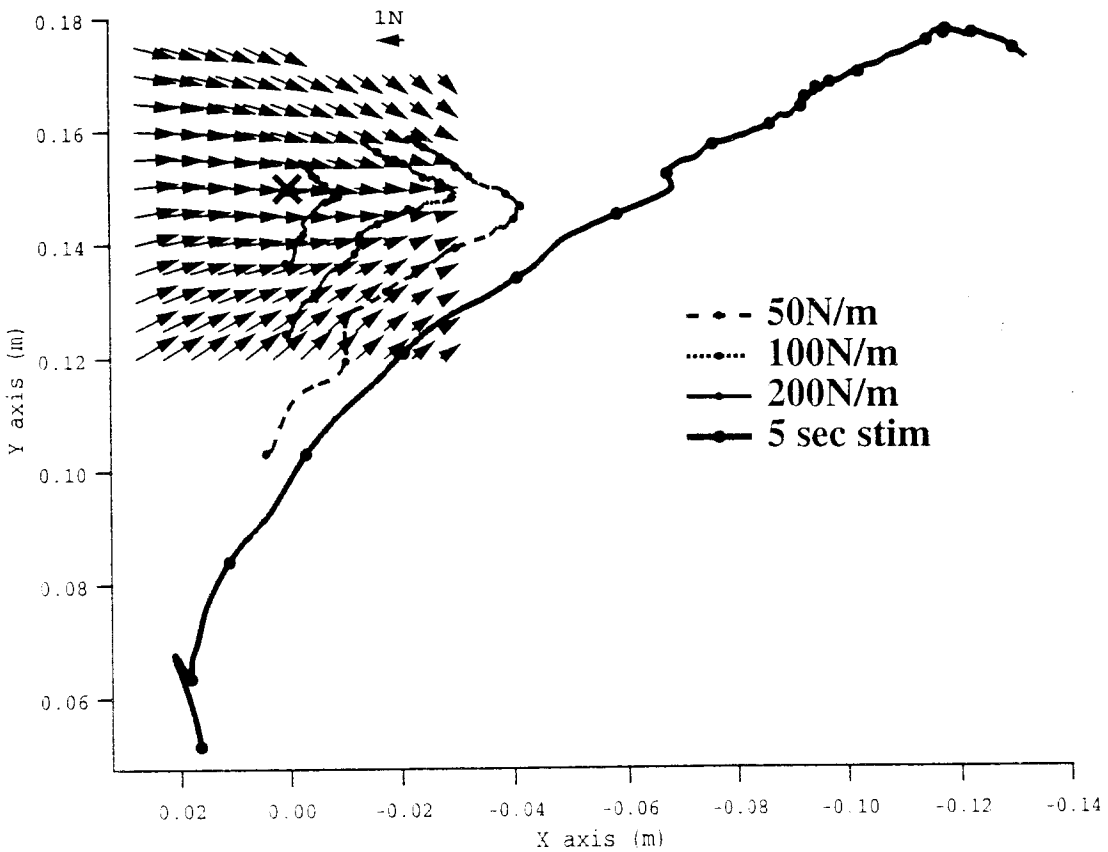

Figure 7.3 Total force field evoked by intraspinal microstimulation with a 0.5 s duration train of pulses, and the motions evoked by stimulating the same spinal site with 3 to 5 s duration trains of pulses. Three of the movements were made against simulated linear spring with increasing stiffness (50-100-200 N/m, 3 s stimulation train, **X** marks the spring's point of attraction), and one of the move was against no external load (5 s stimulation train). The active force field was a flexion withdrawal response, i.e. the active forces pointed upward and backward even in the upper right corner of the force measurement workspace. Since the active forces increase in magnitude with stimulation level but retain the same orientation, the movements presented here are consistent with the force orientation.

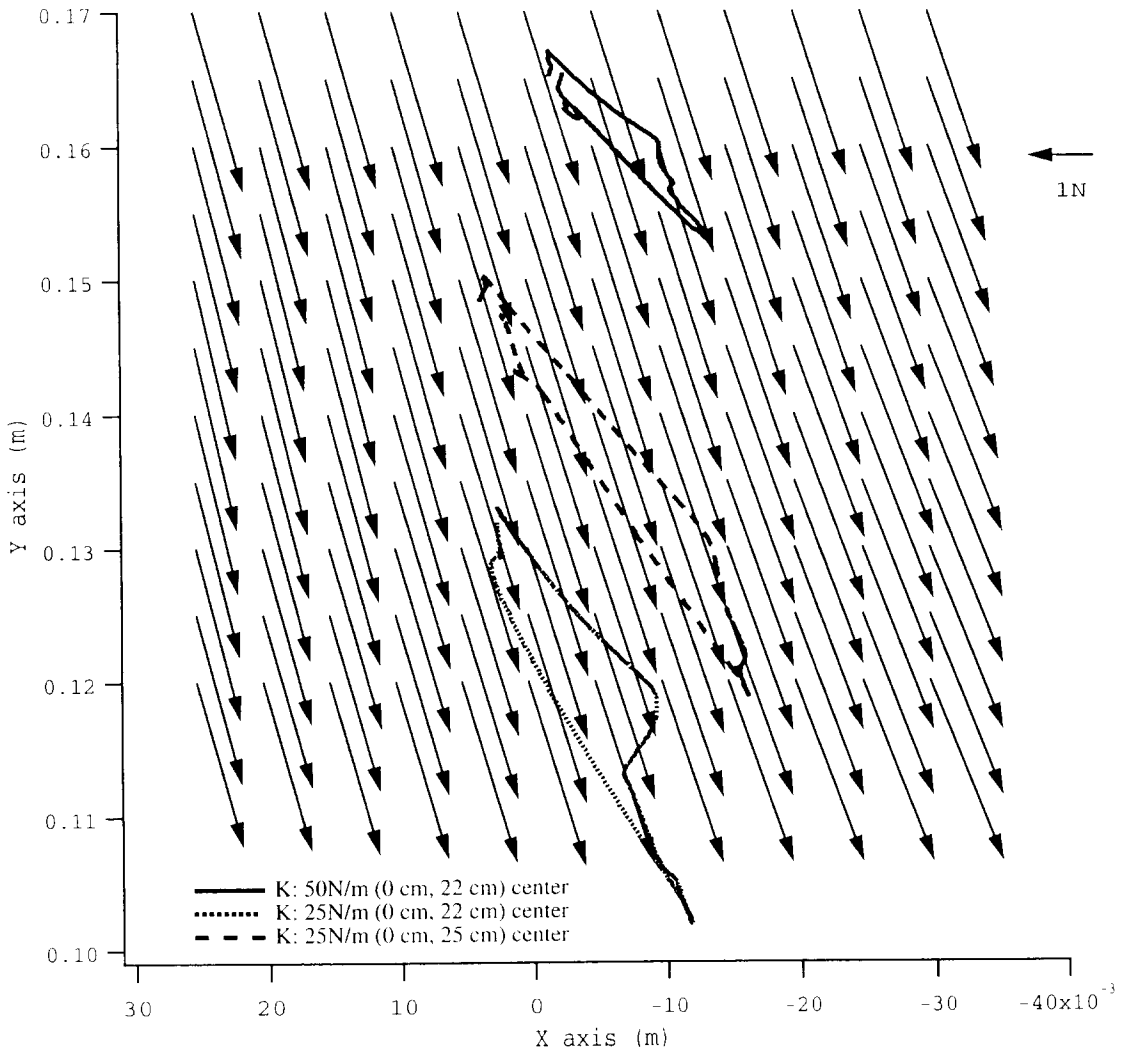

Figure 7.4 Total force field evoked by intraspinal microstimulation with a 0.5 s duration train of pulses, and the motions evoked by stimulating the same spinal site with 3 duration trains of pulses. The three movements were made against simulated linear spring of two stiffnesses (25&50 N/m), with the center point of the 25 N/m spring at (0 cm, 22 cm) and (0 cm, 25 cm) (lower and higher traces respectively). The active force field was a caudal extension response in this case. The limb started at the balance between its own gravity pull, and the restoring force of the spring. The limb then extended caudally with the onset of stimulation, and returned to the starting position once stimulation was turned off. The motion was again consistent with the forces acting on the limb.

CONCLUSIONS

Our measurements of movements in decerebrated, spinal-intact cats indicate that the forces produced by intraspinal microstimulation are large enough to actuate the limb. Stimulation duration must be increased above the 0.5 s used to measure isometric force

pattern but the results indicate that the orientations of the forces are preserved with the increase in stimulation duration. Furthermore, the isometric force field is a good predictor of the direction of the movement generated by the field. Measurements of the forces acting on the end-point characterize the forces acting on the limb throughout its workspace, and can be used to predict the direction of the movements that will be generated by intraspinal microstimulation. Further work on the biomechanics of the limb are required to determine how and if the forces measured isometrically are influenced by movements.

OBJECTIVES FOR THE NEXT QUARTER

In the next quarter we will continue our studies to identify spinal neurons which project to pudendal motoneurons. active during micturition. We will improve identification of the urethral sphincter motor-nucleus location by selective stimulation of the urethral sphincter motor branch of the pudendal nerve. Analysis of the current CTB histological sections, and the retrograde microsphere and CTB labeled neuron locations will be completed in the next quarter.

We will continue our studies characterizing the hindlimb motor responses to lumbar microstimulation. Our objectives for the next quarter are to evaluate the counter-gravity ability of the extensor responses. The robot will be used to simulate a constant force (equivalent to gravity times the mass of the cat divided by four) pushing up against the limb. Our objectives will be to demonstrate that the extensor force pattern can be sufficiently large to extend the limb against such a force.

LITERATURE CITED

Hoover, J.E., R.G. Durkovic (1992) Retrograde labeling of lumbosacral interneurons following injections of red and green flourescent microspheres into hindlimb motor nuclei of the cat. Somatosens. Motor Res. 9:211-226.

Jankowska E, and Riddell JS (1993) A relay for input from group II muscle afferents in sacral segments of the cat spinal cord. J Physiol (Lond) Jun;465:561-80.

Nadelhaft, I, W.C. DeGroat, C. Morgan (1980) Location and morphology of parasympathetic preganglionic neurons in the sacral spinal cord of the cat revealed by retrograde axonal transport of HRP. J. Comp. Neurol. 193:265-286.

Nicholls, J.G., A.R. Martin, B.G. Wallace (1992) From Neuron to Brain. Sinauer Associates, Inc., Sunderland, MA, pg.288-289.

Thor, K.B., C. Morgan, I. Nadelhaft, M. Houston, W.C. de Groat (1989) Organization of afferent and efferent pathways in the pudendal nerve of the female cat. J. Comp. Neurol. 288:263-279.

Ueyama, T. N. Mizuno, S. Nomura, A. Konishi, K. Itoh, H. Arakawa (1984) Central distribution of afferent and efferent components of the pudendal nerve in cat. J. Comp. Neurol. 222:38-46.

Van Buren, J.M., K. Frank (1965) Correlation between the morphology and potential field of a spinal motor nucleus in the cat. Electroenceph. Clin. Neurophys. 19:112-126.

Vanderhorst, V.G.J.M., and Holstege (1997) Organization of lumbosacral motoneuronal cell groups innervating hindlimb, pelvic floor, and axial muscles in the cat. J. Comp. Neurol. 382:46-76.